*Geophys. J. R. astr. Soc.* (1977) 51, 625–651

# High-frequency radiation from crack (stress drop) models of earthquake faulting

Raul Madariaga* *Massachusetts Institute of Technology, Cambridge, Massachusetts 02139, USA*

Received 1977 May 24; in original form 1977 January 11

**Summary.** We present a theory for the radiation of high-frequency waves by earthquake faults. We model the fault as a planar region in which the stress drops to the kinematic friction during slip. This model is entirely equivalent to a shear crack. For two-dimensional fault models we show that the high frequencies originate from the stress and slip velocity concentrations in the vicinity of the fault's edges. These stress concentrations radiate when the crack expands with accelerated motion. The most efficient generation of high-frequency waves occurs when the rupture velocity changes abruptly. In this case, the displacement spectrum has an $\omega^{-2}$ behaviour at high frequencies. The excitation is proportional to the intensity of the stress concentration near the crack tips and to the change in the focusing factor due to rupture velocity. We extend these two-dimensional results to more general three-dimensional fault models in the case when the rupture velocity changes simultaneously on the rupture front. Results are similar to those described for two-dimensional faults. We apply the theory to the case of a circular fault that grows at constant velocity and stops suddenly. The present theory is in excellent agreement with a numerical solution of the same problem.

Our results provide upper bounds to the high-frequency radiation from more realistic models in which rupture velocity does not change suddenly. The $\omega^{-2}$ is the minimum possible decay at high frequencies for any crack model of the source.

## 1 Introduction

One of the least understood problems in the study of earthquake source mechanism is the radiation of high-frequency seismic waves. A model for the generation of these waves is crucial in order to predict strong motion in the frequency range of interest to engineering (1–20 Hz). The kinematic models (Haskell 1964; Savage 1966) used by seismologists are low-frequency models that tend to average out the details of the slip function at the source.

*Present address: Institut de Physique du Globe, University of Paris VI, 75230 Paris, Cedex 05, France.

Moreover, because these models assume constant slip on the fault there are unphysical stress singularities near the edges of the fault. These singularities are the most important feature of the stress field and we may expect that they control the high-frequency radiation. In the constant dislocation models these singularities are not integrable and they generate an infinite strain energy flow into the rupture front. Stress relaxation models (finite stress drop or shear crack models) still retain singularities in the elastic stress field (Kostrov 1964; Burridge 1969; Brune 1970; Dahlen 1974; Richards 1976; Madariaga 1976). However, as shown by Kostrov, Nikitin & Flitman (1970) and Freund (1972b) the energy flow into the rupture front is finite and is physically associated with the energy necessary to fracture the material on the fault surface. The singularities in this case are a consequence of the use of linear elasticity even in the vicinity of the rupture front. These singularities would disappear if nonlinear effects near the rupture front were taken into account.

Ideally it may be possible to study high-frequency radiation solving models with physically reasonable stress drop distributions on the fault. Unfortunately such models may be studied only with numerical methods which become extremely expensive as the frequency increases. Even if it were possible to solve these models it would be important to have a physical understanding of the behaviour of high frequencies. The aim should be to obtain simple releations similar to the one between low-frequency spectral amplitude and the seismic moment (Aki 1967). Such simple relations are very unlikely, however, since high-frequency radiation should be highly incoherent due to the inhomogeneity of stress and strength (fracture energy) on the fault. Attempts to describe the incoherence of the radiation were made by Haskell (1966) and Aki (1967) based on intuitive considerations about slip correlation. Our effort here is different, since we shall try to isolate the source of high-frequency radiation and to describe its dynamic characteristics. This study was prompted by the observation that in all the deterministic source models – dislocation or crack – studied by seismologists, the high-frequency radiation is determined by starting and stopping phases radiated by abrupt rupture velocity changes at the fault. We show here that the high-frequency radiation from crack – or stress drop – models is proportional to the stress concentrations at the rupture fronts.

## 2 General properties of shear faults

We model an earthquake as the rapid spreading of rupture on a plane fault whose sides slip due to the inability of the fault to support the tectonic shear stress. When the tectonic stress overcomes the static friction or strength of the rock the fault starts to slip and the stress drops more or less abruptly to the kinetic friction. The stress drop on the fault generates large stress concentrations near the edge of the fault which will tend to spread the fault. The rupture process may be stable as in fault creep or unstable as in earthquakes depending on the available energy, non-elastic material properties, pore fluids, etc. (Rice & Simons 1976). Since we are interested in seismic radiation we consider only unstable or brittle ruptures. The instability appears because as the crack extends the stress concentrations tend to become larger causing simultaneously an increase in the rupture velocity. Once rupture is initiated the rupture velocity tends to accelerate up to the shear velocity for antiplane cracks (Kostrov 1966) or the Rayleigh velocity for in plane shear cracks (Fossum & Freund 1975). Some models proposed by Burridge (1973), Andrews (1976) and Das (1976) also allow for transonic rupture velocities.

The stress concentrations in the vicinity of the rupture front are of course finite and controlled by the nonlinear material properties of the rocks or the fault gouge. To study problems that incorporate nonlinear material behaviour is extremely difficult. However, it

is well known in fracture mechanics (Rice 1968) that the behaviour of cracks may be approximated assuming (1) that the material is elastic everywhere, even in the vicinity of the crack tip and (2) that the stress drops to the kinetic friction immediately behind the rupture front. A consequence of these assumptions is that the stress concentration becomes singular and has the general form

$$\sigma = K_d\,[x - \xi(t)]^{-1/2} \quad \text{for} \quad x > \xi(t) \tag{1}$$

where $\xi(t)$ is the current location of the crack tip, $x$ is the coordinate along the fault plane, $K_d$ is the dynamic stress intensity factor. Referring to the coordinates in Fig. 1, the stress $\sigma = \sigma_{xz}$ for in plane shear and $\sigma = \sigma_{xy}$ for antiplane shear. Although the stress appears to be infinite at the crack tip, the stress distribution (1) is valid only outside some small inelastic zone surrounding the crack tip. Inside this core zone either one or both of the assumptions above fails. For brittle fractures the size of the inelastic zone is usually very small compared to any of the fault dimensions. There are two scales in the problem so that we may solve the elastic external problem using only global properties of the nonlinear inner problem. The inelastic zone is almost certainly very small in earthquakes since we expect it to be of the order of the width of the gauge. In order to compute high-frequency radiation the elastic approximation is sufficient since the wavelengths of interest ($\lambda > 100$ m at about 20 Hz) are much larger than the size of the gouge (at most a few metres). The radiation at these wavelengths should be insensitive to details of the inelastic zone.

When the rupture front is moving the dynamic stress intensity factor $K_d$ may be separated into two terms (Eshelby 1969; Fossum & Freund 1975; Freund 1976)

$$K_d = A(v_R)K^*(\xi, t) \tag{2}$$

where

$$A(v_R) = (1 - v_R/v_S)^{1/2}$$

for antiplane cracks and

$$A(v_R) = S(-1/v_R)\,\frac{(1 - v_R/c_R)}{(1 - v_R/v_S)^{1/2}}$$

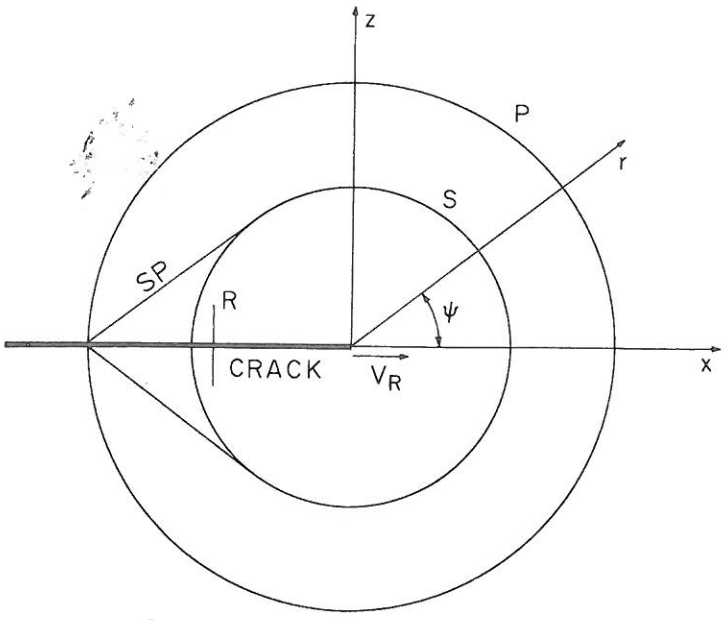


**Figure 1.** Geometry of the two-dimensional fault in the vicinity of the crack tip and wavefronts of the in-plane problem. R indicates the Rayleigh wave propagating along the cracked portion of the fault.

for plane cracks. Here $v_R$ is the instantaneous rupture velocity, $v_P$, $v_S$ and $c_R$ are the $P$, $S$ and Rayleigh wave velocities, respectively and $S(p)$ is the de Hoop (1958) function defined in the Appendix 1. The stress intensity $K^*$ may be interpreted as the stress concentration that would remain if the crack suddenly stopped: it is a function only of the stress and extension history of the fault but it is independent of the instantaneous rupture velocity $v_R$. The velocity factor $A(v_R)$, on the other hand, depends only on $v_R$. It decreases monotonically from 1 at $v_R = 0$ to 0 at the terminal velocity ($v_S$ for antiplane cracks and $c_R$ for plane cracks).

Closely connected with the stress concentration outside the crack there is a singularity in slip velocity ($\dot{D}_x$ for plane, $\dot{D}_y$ for antiplane cracks) immediately behind the rupture front. This singularity is of the form

$$\dot{D} = V_d [\xi(t) - x]^{-1/2} \text{ for } x < \xi(t) \tag{3}$$

where

$$V_d = 2\frac{K^*}{\mu} v_R B(v_R) \tag{4}$$

$$B(v_R) = (1 + v_R/v_S)^{-1/2}$$

for antiplane cracks, and

$$B(v_R) = \frac{\kappa^2}{2(\kappa^2 - 1)} \frac{(1 + v_R/v_S)^{1/2}}{(1 + v_R/c_R) S(1/v_R)}$$

for plane cracks. $\kappa = v_P/v_S$ and $\mu$ is the rigidity. $B(v_R)$ depends only on the instantaneous rupture velocity. $V_d$ goes to zero when $v_R$ goes to zero and is finite for all other rupture velocities.

A final physical property of interest is the energy absorption per unit advance of the crack which is usually called the energy release rate. This is that part of strain energy released by the body that is available at the crack tip to be used to fracture the material. Using some results by Achenbach (1974) we find

$$G = \frac{(K^*)^2}{\mu} A(v_R) B(v_R) \tag{5}$$

where $A(v_R)$ $B(v_R)$ is a function only of the rupture velocity that decreases from a value near 1 at $v_R = 0$ to zero at the terminal velocity. If as usual we define $\gamma$ – the specific fracture energy – as the energy necessary to create a unit surface of fresh crack, then the energy balance at the rupture front is

$$2\gamma = G \tag{6}$$

given $\gamma$, which is a property of the material, this is an equation for the instantaneous rupture velocity.

A notable property of the previous results is that the dynamic field near the tip depends on the stress history and the rupture velocity but is independent of the rupture acceleration. This surprising property, first noticed by Eshelby (1969), implies that when a rupture front encounters a sudden change in the fracture energy of the material, for instance when rupture penetrates into different material, the rupture velocity changes abruptly. An extreme case is the unbreakable barrier considered by Husseini *et al.* (1975) where rupture will be abruptly stopped. The intense radiation generated by this event is usually called a stopping phase.

High-frequency radiation is determined by the slip velocity field at the source. Since the highest slip velocities occur right behind the rupture front we may expect that the radiation of high-frequency seismic waves be controlled by the motion and intensity of the slip velocity concentrations. By high frequencies we mean wavelengths smaller than the geometrical dimensions of the fault and larger than the nonlinear zone near the rupture front. We may think of the rupture front as a moving line source whose strength, given by $V_d$ (4), depends on the load history and the instantaneous rupture velocity. When the rupture velocity is constant, the velocity intensity $V_d$ changes only due to the slow continuous variation in $K^*$ and there is practically no high-frequency radiation by the rupture front. On the other hand, strong radiation occurs when the rupture velocity changes abruptly. In this case the stress intensity $K_d$ and velocity intensity $V_d$ also change abruptly generating a strong discontinuous wave front. High frequencies are associated with these discontinuities in the radiation. If the rupture accelerates or decelerates continuously, radiation will also be emitted continuously. At frequencies such that the period is longer than the total acceleration time the radiation will approach that of an abrupt velocity change, while at shorter periods the motion of the rupture front appears to be smooth and the radiation is less efficient. Thus, the radiation from velocity jumps provides upper bounds to the high-frequency radiation. A proof of this hypothesis for faults of general geometry is extremely difficult. Instead we study first simpler two-dimensional models both in plane and antiplane strain. Later we shall use the fact that the elastic field is very approximately two-dimensional near the rupture front to extend these results to three dimensions.

## 3 Sudden start of an antiplane shear rupture

Perhaps the simplest transient crack model is the sudden extension of a pre-existing antiplane crack. Although this model is too simple to be directly applicable to earthquakes, we shall show later that many features of the seismic radiation from this model apply to more realistic fault models. We consider the following problem, for time $t < 0$ a static antiplane crack extends from the origin along the negative $x$ axis as shown in Fig. 2(a). The body is loaded by a certain static stress field away from the crack. The crack has slipped and the stress at the fault has relaxed to the kinetic friction. Due to this stress drop there is a stress concentration.

$$\sigma_{xy} = K_0 x^{-1/2} \quad x > 0 \tag{7}$$

along the $x$ axis in front of the crack (Fig. 2). This stress concentration is measured from the stress level right behind the crack tip, so that in order to study the elastodynamic field in the vicinity of the crack tip we may choose as stress reference level the kinetic friction on the fault. At time $t = 0$ the crack starts to extend at a constant subsonic velocity $v_R$. We want to find the waves emitted by the sudden start of the crack. Since we are interested primarily on the high-frequency radiation we only have to be concerned with the field in the vicinity of the crack tip. We notice, finally, that the stress intensity factor $K_0$ contains all the information about the loading stress and the size of the fault that is necessary to solve the problem.

As the crack extends it 'absorbs' the singular static stress field in front of the tip. That is, as shown in Fig. 2, the stress drop is minus the stress concentration (7). In order to find the radiation of elastic waves we first have to solve a crack problem to find the dynamic stresses outside the crack and the slip velocity on the crack. A general solution to antiplane crack problems was found by Kostrov (1966). He showed that the stress change on the plane of the fault, ahead of the crack tip, is given in terms of the stress drop $\Delta\sigma$ inside the crack by

$$\sigma_{xy}(x, 0, t) = \frac{1}{\pi(x-l)^{1/2}} \int_{x-v_S t}^{l} \Delta\sigma_{xy}(\xi) \frac{(l-\xi)^{1/2}}{x-\xi} d\xi \tag{8}$$

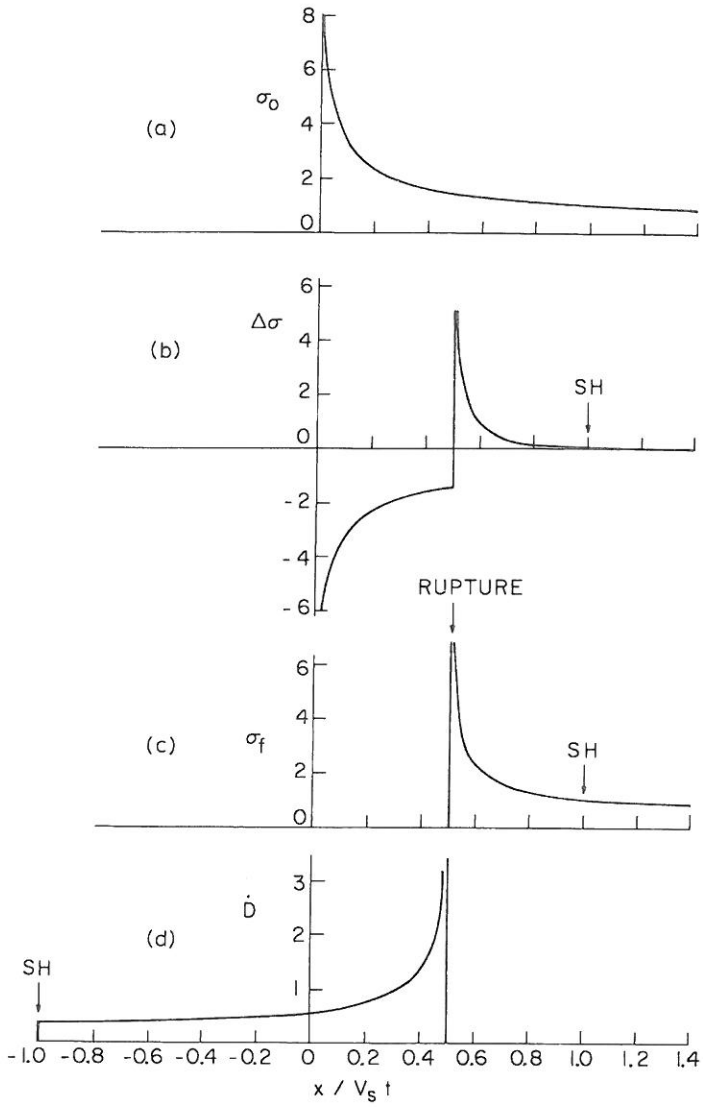


**Figure 2.** The elastic field on the plane of a suddenly starting antiplane crack with rupture velocity $v_R = 0.5\, v_S$. (a) Shows the state of stress immediately before the rupture starting. (b) Stress change on the fault plane due to rupture propagation. The stress drop inside the crack is non-uniform and equal to the pre-stress of the upper figure. Ahead of the rupture there is a stress increase. (c) The total stress $\sigma_f = \sigma_0 + \Delta\sigma$ on the fault plane. The crack is stress free and there is a stress concentration ahead of the rupture front. (d) The slip velocity distribution on the fault.

where $l = l(x, t)$ is the retarded location of the crack tip, which in the specific case of a crack that grows at a constant rupture velocity is given by

$$l(x, t) = (v_S t - x)/(v_S/v_R - 1).$$

The stress drop inside the crack is

$$\Delta\sigma_{xy}(x, 0, t) = -\frac{K_0}{x^{1/2}}, \quad 0 < x < v_R t \tag{9}$$

so that inserting it in (8) and integrating we find

$$\sigma_{xy}(x, 0, t) = -\frac{K_0}{x^{1/2}} + K_0 \frac{(1 - v_R/v_S)^{1/2}}{(x - v_R t)^{1/2}}, \quad v_S t > x > v_R t \tag{10}$$

on the continuation of the fault. The stress change on the plane of the fault (9, 10) is shown in Fig. 2(b). In order to find the total stress field we have to add the initial stress field (7). We find

$$\begin{aligned} \sigma_{xy}(x, 0, t) &= 0 && x < v_R t \\ &= K_d (x - v_R t)^{-1/2} && v_R t < x < v_S t \\ &= K_0 x^{-1/2} && x > v_S t. \end{aligned} \tag{11}$$

This stress distribution is shown in Fig. 2(c). We notice that the stress has a moving singularity at the rupture front ($x = v_R t$). The intensity of this singularity is $K_d = K_0 A(v_R)$ in agreement with the general properties discussed in the previous section (equation 2) with $K^* = K_0$. Thus when the rupture starts the stress intensity drops abruptly from $K_0$ to $K_d$. It is this change in stress intensity that causes the radiation of discontinuous wave fronts. The discontinuous wave front appears in the form of a slope discontinuity in stress that propagates with the shear wave velocity – see Fig. 2(c).

Using Kostrov's method it is also possible to find the slip velocity $\dot{D}_y$ on the fault (Achenbach 1974). The final result in our problem is

$$\dot{D}_y(x, 0, t) = 2 \frac{K_0}{\mu} v_R \, (1 + v_R/v_S)^{-1/2} \cdot (v_R t - x)^{-1/2}, \quad -v_S t < x < v_R t. \tag{12}$$

The slip velocity is singular at the rupture front ($x = v_R t$) and the velocity intensity is precisely of the general form given in equation (4). The slip velocity has a step-like discontinuity that moves with the $S$-wave velocity.

We may now find the radiation using the slip velocity function (12) as a dislocation velocity in a representation theorem. This method requires rather complicated integrations so that it is preferable to use Laplace transforms. Let us introduce the following double transform of the displacement

$$u_y(p, z, s) = \int_0^\infty \exp(-st)\, dt \int_{-\infty}^\infty u_y(x, z, t) \exp(-spx) dp \tag{13}$$

We can then write the doubly transformed representation theorem in the simple form

$$\dot{u}_y(p, z, s) = 1/2 \, \dot{D}_y(p, 0, s) \exp(-s\gamma_S z) \tag{14}$$

where $\gamma_S = (1/v_S^2 - p^2)^{1/2}$ and $\dot{D}_y(p, 0, s)$ is the doubly transformed slip velocity function (12). By straightforward application of Laplace transforms we find

$$\dot{u}_y(p, z, s) = \frac{K_0 \, \pi^{1/2}}{\mu \; s^{3/2}} \frac{1}{(1/v_S - p)^{1/2} (1/v_R + p)} \exp(-s\gamma_S z) \tag{15}$$

where $\dot{u}_y$ is the particle velocity field. The inverse of (15) to the time domain may be found by means of the Cagniard–de Hoop technique (Achenbach 1975, p. 298). The result is

$$\dot{u}_y(x, z, t) = \frac{K_0}{\mu} v_S \frac{1}{r^{1/2}} \cdot \frac{1}{\pi} \int_1^{t'} \mathrm{Re} \left[ \frac{(1+p)^{1/2}}{M+p} \right] \frac{d\tau}{\sqrt{t' - \tau} \sqrt{\tau^2 - 1}} \tag{16}$$

where $r$, $\psi$ are the cylindrical coordinates shown in Fig. 1, $M = v_S/v_R$, $p(\tau)$ is the Cagniard contour

$$p(\tau) = -\tau \cos\psi + i\sqrt{\tau^2 - 1} \sin\psi, \quad -\pi \leq \psi \leq \pi$$

and $t' = v_S t/r$ is the non-dimensional time. The numerical evaluation of the integral in (16) is straightforward if proper care is taken of the singularities (Acton 1970, p. 414). In Fig. 3 we show the radiation in several directions $\psi$ as a function on non-dimensional time. The most significant feature of the particle velocity is the discontinuity on the *SH*-wave front. In the forward direction $\psi \approx 0$ there is also a strong velocity peak associated with the slip velocity singularity at the rupture front. This is a near field effect that appears only in the vicinity of the rupture front. In all other directions the particle velocity field is dominated by the velocity jump on the wave front. The velocity jump is given by

$$\dot{u}_y(x, z, t) = \frac{K_0}{\mu} v_R r^{-1/2} \frac{\sin \psi/2}{1 - v_R/v_S \cos \psi}. \tag{17}$$

Further study of this discontinuity is deferred to Section 5.

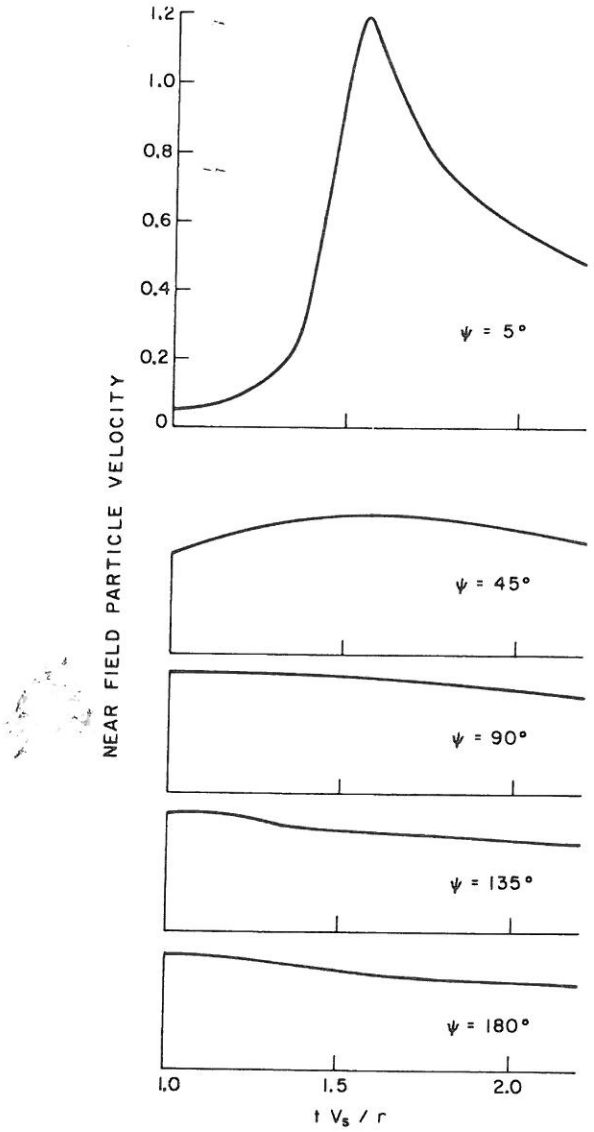


**Figure 3.** Near field of the suddenly starting antiplane crack in different directions $\psi$. The velocity field has step discontinuities on the *SH*-wave front. The peak at $\psi = 5°$ is due to the passage of the rupture front.

## 4 Sudden start of a plane rupture

We study again the problem of the previous section but for an in-plane shear crack. A static plane shear crack extends along the negative $x$ axis. The stress inside the crack is relaxed to the kinetic friction level which is used as the reference stress level. Outside the crack, on its own plane, there is a stress singularity $\sigma_{xy} = K_0 x^{-1/2}$ where the stress is measured from the kinetic friction level. At time $t = 0$ the crack suddenly starts to grow with a constant rupture velocity $v_R$. In the new crack surface the stress drop is

$$\Delta\sigma_{xz} = -K_0 x^{-1/2} \qquad 0 < x < v_R t. \tag{18}$$

We have to solve a crack problem to find the stress change outside the crack and the slip velocity on the fault. This problem was solved by Fossum & Freund (1975) using methods developed by Freund (1972a). In the following we shall use the somewhat simpler method proposed by Kostrov (1975) which allows for variable rupture velocities and time-dependent stress drops. We introduce double Laplace transforms of all the field variables as in (13). From the elastic wave equation and symmetry about $z = 0$, the stress and displacement on the plane of the fault ($z = 0$) are related by

$$\sigma_{xz}(p, 0, s) = -\mu v_S^2 \frac{R(p)}{\gamma_S} u_x(p, 0, s) \tag{19}$$

where

$$R(p) = (1/2\, v_S^{-2} - p^2)^2 + p^2 \gamma_P \gamma_S \tag{20}$$

is the Rayleigh function and

$$\gamma_P = (v_P^{-2} - p^2)^{1/2}$$

$$\gamma_S = (v_S^{-2} - p^2)^{1/2}$$

$v_P$ and $v_S$ are the $P$- and $S$-wave velocities respectively and $\mu$ is the rigidity. The problem consists in finding the stress outside the fault given the stress drop inside the fault and that there is no slip outside the fault. This mixed boundary problem is complicated by the presence of the Rayleigh function in (19). Kostrov's method consists in transforming equation (19) into another equation which is easier to solve. The first step is to use de Hoop's (1958) decomposition of the Rayleigh function into forward and backward waves

$$R(p) = \frac{(\kappa^2 - 1)}{2v_P^2} \left(\frac{1}{c_R} - p\right) S(-p) \left(\frac{1}{c_R} + p\right) S(p) \tag{21}$$

where $c_R$ is the Rayleigh wave velocity, $\kappa = v_P/v_S$ and $S(p)$ is the de Hoop function defined in the Appendix I. The function $(c_R^{-1} + p)\, S(p)$ is analytic in the complex half-plane $\mathrm{Re}\, p > -v_P^{-1}$ so that it represents only waves travelling in the forward directions ($|\psi| < 90°$ referring to Fig. 1. Conversely $(c_R^{-1} - p)\, S(-p)$ is analytic in $\mathrm{Re}\, p < v_P^{-1}$ and represents waves in the backward direction ($|\psi| > 90°$).

Let us define the pseudostress

$$\Sigma(p, s) = \frac{\gamma_P^+ \gamma_S^+}{(c_R^{-1} + p) S(p)} \sigma_{xz}(p, 0, s) \tag{22}$$

and the pseudoslip

$$\Delta(p, s) = \frac{(\kappa^2 - 1)}{\kappa^2} \frac{(c_R^{-1} - p) S(-p)}{\gamma_P^- \gamma_S^-} D_x(p, 0, s) \tag{23}$$

where

$$\gamma_P^{\pm} = (1/v_P \pm p)^{1/2}$$

and

$$\gamma_S^{\pm} = (1/v_S \pm p)^{1/2}.$$

The definition (23) differs by a constant factor from Kostrov's because of a misprint in his paper. From (19) we find now

$$\Sigma(p, s) + \mu s \gamma_P^{+} \gamma_P^{-} \Delta(p, s) = 0. \tag{24}$$

This equation may be inverted immediately to

$$\Delta(x, t) = -\frac{1}{\mu\pi} \iint \frac{\Sigma(\xi, \tau)\, d\xi\, d\tau}{[(t-\tau)^2 - (x-\xi)^2/v_P^2]^{1/2}} \tag{25}$$

where the double integral is taken on the triangular zone

$$|v_P(t-\tau)| > |(x-\xi)|, \quad t > 0.$$

Equation (25) has exactly the same form as the antiplane representation theorem (Kostrov 1966) except that the $P$-wave velocity $v_P$ replaces $v_S$ in the latter. In order to solve the crack problem we still have to find the boundary conditions for $\Sigma$ and $\Delta$. For the pseudoslip it is simply $\Delta(x_0, t_0) = 0$ for points ahead of the rupture front. For the pseudo-stress drop we have to solve some unwieldy integrals given by Kostrov (1975). However, the stress drop (18) is time-independent and in this case Kostrov showed that $\Sigma(x, \tau) = \Delta\sigma(x)$. The integral equation that has to be solved is of the same form as that solved for antiplane problems. Using the methods of the previous section we find the pseudo-stress outside the crack

$$\Sigma(x, t) = -K_0 x^{1/2} + K_0 \frac{(1 - v_R/v_P)^{1/2}}{(x - v_R t)}, \quad v_R t < x < v_P t. \tag{26}$$

Since inside the crack $\Sigma(x, t)$ is given by (18) we can obtain the transform of $\Sigma(x, t)$

$$\Sigma(p, s) = -K_0 \frac{\pi^{1/2}}{s^{3/2}} \frac{(v_P^{-1} + p)^{1/2}}{v_R^{-1} + p}. \tag{27}$$

It is now a simple matter to find $\sigma_{xz}$ from (22)

$$\sigma_{xz}(p, 0, s) = -K_0 \frac{\pi^{1/2}}{s^{3/2}} \frac{(c_R^{-1} + p) S(p)}{(v_S^{-1} + p)^{1/2} (v_R^{-1} + p)}. \tag{28}$$

The inversion of (28) may be obtained by a Cagniard–de Hoop inversion

$$\sigma_{xz}(x, 0, t) = K_0 x^{-1/2} T\left(\frac{v_P t}{x}\right) \quad x > 0 \tag{29}$$

where the non-dimensional function $T(\tau)$ is defined in the Appendix 2. The stress change $\sigma_{xz}$ is shown in Fig. 4(b). In order to find the total stress field we add the initial stress field. The total field is shown in Fig. 4(c). The stress field has a singularity of the form $\sigma_{xz} = K_d (x - v_R t)^{-1/2}$ at the rupture front. The dynamic stress concentration is given by the relation (2) $K^* = K_0$. Thus, when the rupture starts the stress intensity drops from $K_0$ to $K_d$. This jump in intensity generates discontinuous wave fronts. The stress field of Fig. 4(c) has a slope discontinuity at the $P$-wave front and a sudden drop in stress at the shear-wave

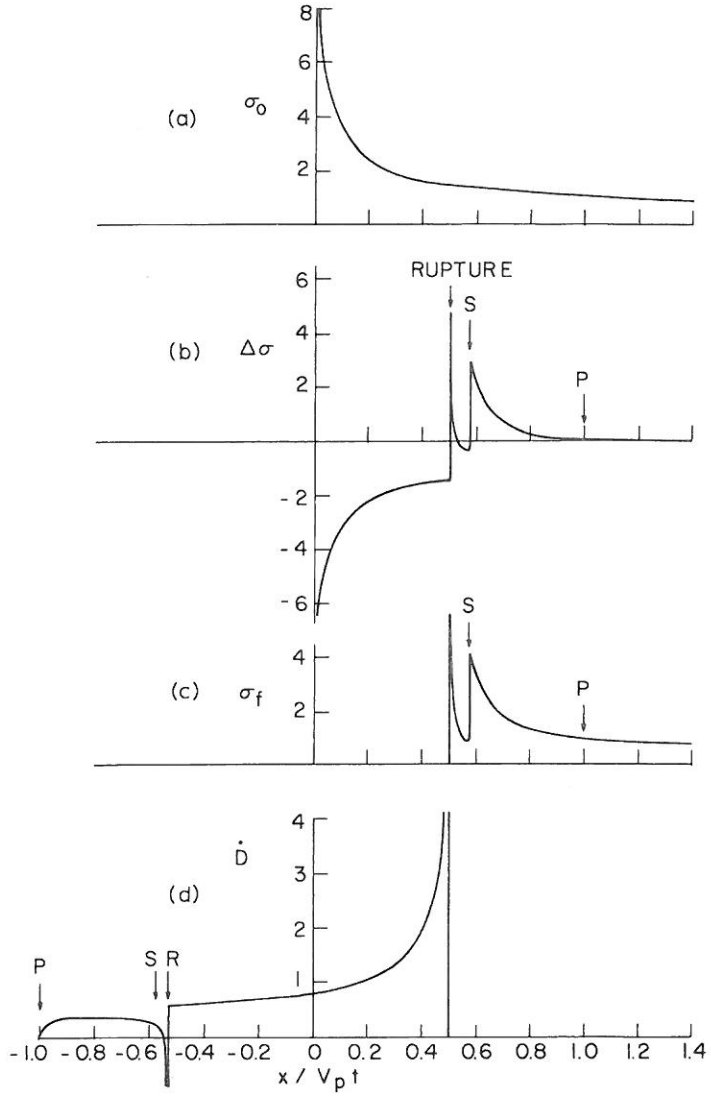


**Figure 4.** The elastic field on the plane of a suddenly starting in-plane shear crack. Rupture velocity $v_R = 0.9\, v_S$. (a) Is the static field before rupture initiation. (b) Shows the stress change $\Delta\sigma$ due to crack extension. The stress drops inside the crack and increases ahead of the crack. (c) Total stress on the fault during rupture propagation. (d) Slip velocity on the fault plane. *P*, *S* and R designate the *P*, *S* and Rayleigh waves respectively.

front. It is interesting to note that the shear stress is at a maximum just before the arrival of *S* waves. This stress increase is of the same sign necessary to fracture the material. Andrews (1976) and Das (1976) have proposed models in which this stress may be sufficient to cause rupture in front of the *S*-wave front. In this case the rupture velocity may appear to be larger than the shear velocity.

We may now find the transformed slip function inside the crack

$$D_x(p, s) = \frac{K_0}{\mu} \frac{\kappa^2}{(\kappa^2-1)} \frac{\pi^{1/2}}{s^{3/2}} \frac{(v_S^{-1} - p)^{1/2}}{(v_R^{-1} + p)(c_R^{-1} - p) S(p)} \tag{30}$$

from which we invert

$$\dot{D}_x(x, 0, t) = \frac{K_0}{\mu} v_P \frac{\kappa^2}{(\kappa^2-1)} \frac{1}{|x|^{1/2}} U\left(\frac{v_P t}{|x|}\right) \tag{31}$$

where $U(\tau)$ is given in Appendix 3. The slip velocity on the crack is shown in Fig. 4 for the case of a high subsonic velocity $v_R = 0.5\, v_P$. The most noticeable feature of the slip velocity is the presence of two square root singularities. One of these is the expected singularity behind the rupture front whose intensity is given by the general result (4) with $K^* = K_0$. The other singularity is given by

$$\dot{D}_x(x, 0, t) \to -\frac{K_0}{\mu} v_R \frac{\kappa^2}{(\kappa^2-1)} \frac{(1 - c_R/v_S)^{1/2}}{(1 + v_R/c_R) S(-1/c_R)} \frac{1}{(|x| - c_R t)^{1/2}}$$

This singularity is the Rayleigh wave that propagates inside the crack. This Rayleigh wave appears because the boundary condition inside the crack is of the fixed stress type. The arrival of $P$ and $S$ waves are marked by slope discontinuities in the slip velocity field.

The final step is to find the radiation away from the fault. This may be done using the representation theorem, we find

$$\dot{u}_x(p, z, s) = -\frac{v_S^2}{2} \dot{D}(p, s) \left[-2p^2 \exp(-s\gamma_P z) - (v_S^{-2} - 2p^2) \exp(-s\gamma_S z)\right]$$

$$\dot{u}_z(p, z, s) = -\frac{v_S^2}{2} \dot{D}(p, s) \left[2p\gamma_P \exp(-sz\gamma_P) - \frac{(v_S^{-2} - 2p^2)}{\gamma_S} p \exp(-s\gamma_S z)\right]. \tag{32}$$

The inversion of these functions is complicated by the presence of several singularities on the complex-$p$ plane. Using the Cagniard--de Hoop method the particle velocities may be written in the form

$$\dot{u}_i = \frac{K_0}{\mu} v_P \frac{1}{r^{1/2}} V_i\left(\frac{v_P t}{r}, \psi\right), \quad -\pi \leqslant \psi \leqslant \pi \tag{33}$$

where $(r, \psi)$ are polar coordinates as in Fig. 1, $i = x, z$ and the functions $V_i(\tau, \psi)$ are given in Appendix 4. In Fig. 5 we show $V_i$ for several selected directions $\psi$. In the forward direction, for $|\psi| \sim 0$, the dominating features are the high particle velocities near the rupture front. As we move away from the fault plane the discontinuities at the wave fronts dominate the field. In the region $\cos\psi > -v_S/v_P = \kappa^{-1}$ ($|\psi| < 135°$ for $\kappa = 3^{1/2}$) there are jump discontinuities in particle velocity both at the $P$- and $S$-wave fronts. The strength of the jumps is larger in the forward direction due to the focusing effects of rupture. The discontinuities are also modulated by the radiation pattern. For $\cos\psi < -\kappa^{-1}$ an $SP$ wave guided by the crack appears and a logarithmic pulse accompanies the jump discontinuity at the $S$-wave front. Just as with Rayleigh waves the crack acts like a free surface guiding inhomogeneous waves. In spite of all this complexity the radiation in the backward direction is dominated by the $P$- and $S$-wave fronts. The $SP$ wave is a conical wave (see Fig. 1) with a slope discontinuity in its wave front which is weaker than the jump discontinuities or logarithmic pulses of the $P$ and $S$ waves. Furthermore the $SP$ waves are strictly near field phases which are totally diffracted by the other edge of the fault. In practice then they might be observed in a very narrow zone around $\cos\psi = -\kappa^{-1}$.

## 5 Starting phases from plane and antiplane cracks

The near-field solutions of the last two sections have jump discontinuities or logarithmic singularities in particle velocity at the $P$- and $S$-wave fronts. High-frequency radiation is associated with the first motions at these wave fronts. Let us consider first the case of the

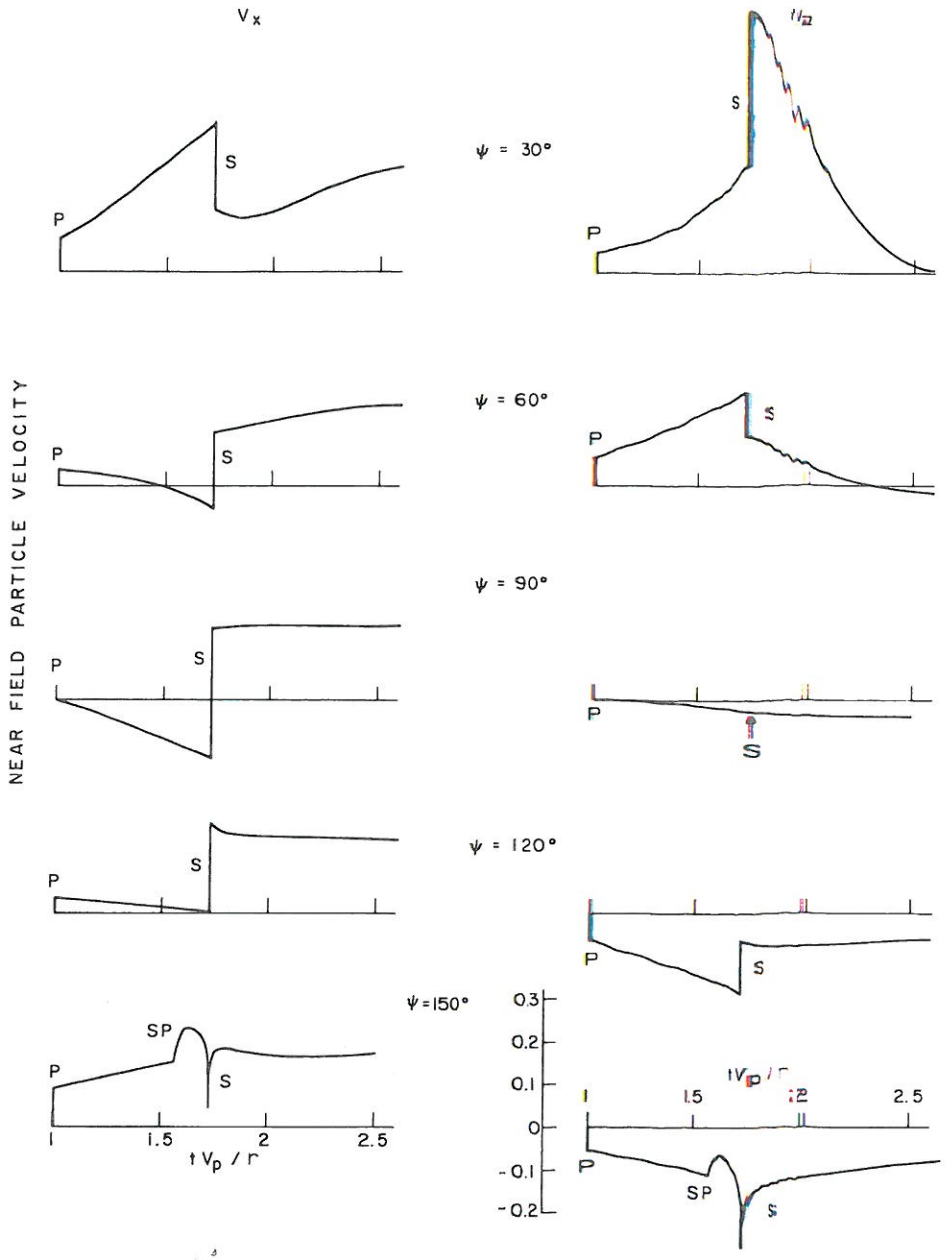


**Figure 5.** Near-field radiation from a suddenly starting in plane shear crack. Rupture velocity $v_R = 0.9\, v_S$. The left column shows the horizontal particle velocity field. The right column shows the vertical particle velocities at different angles of radiation $\psi$. The large particle velocities in the forward direction $\psi = 30°$ are due to focusing effects.

*SH*-starting phases radiated by a suddenly starting antiplane crack. The first motion may be found from (16) when $t' \to 1$

$$u_y(r, \psi, t) = \frac{K_0}{\mu} v_R \frac{1}{r^{1/2}} \frac{\sin \psi/2}{1 - (v_R/v_S)\cos \psi} H(t - r/v_S). \tag{34}$$

Thus, the starting phase is a jump in velocity which is proportional to the stress concentration $K_0$ before the crack starts to move. It has the typical $r^{-1/2}$ geometrical spreading factor of cylindrical waves. The radiation pattern, shown in Fig. 6 for the case $v_R = 0.87\, v_S$, includes in the denominator the factor $(1 - (v_R/v_S)\cos \psi)$ which accounts for the focusing of radiation in the direction of rupture propagation. This factor is the same as that found by

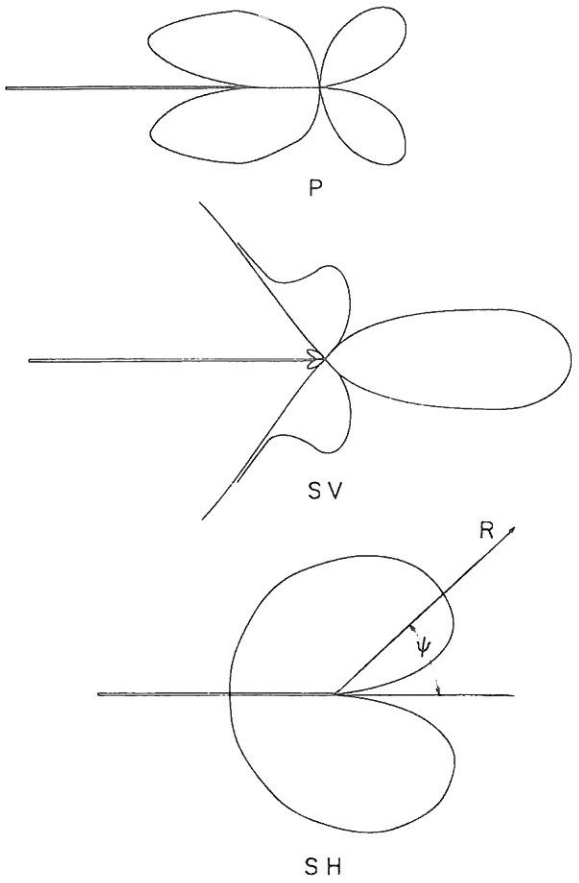


**Figure 6.** Radiation patterns from the suddenly starting or stopping in plane shear crack (*P* and *SV* waves) and a sudden starting or stopping antiplane crack (*SH* waves).

Ben-Menahem (1962) for moving point sources. The radiation pattern differs from that of a dislocation which is simply $\sin\psi$. The most important difference is that $\psi = \pi$, i.e. the direction towards the crack, is not a nodal line for a crack.

The first motion or starting phases from the in-plane shear crack may be found from (33) and the function $V_i(\tau, \psi)$ defined in Appendix 4. For *P* waves the first motion is

$$\dot{u}_r^P(r, \psi, t) = \frac{K_0}{\mu} v_R \frac{1}{r^{1/2}} \frac{\sin 2\psi}{1 - v_R/v_P \cos\psi} F_P(\psi) H(t - r/v_P) \tag{35}$$

where the factor

$$F_P(\psi) = \frac{1}{2^{3/2}(\kappa^2 - 1)} \frac{(\kappa + \cos\psi)^{1/2}}{(q_R + \cos\psi) S(\cos\psi/v_P)}$$

modifies the radiation pattern $\sin 2\psi$ from an edge dislocation, $q_R = c_R/v_P$ and the denominator $(1 - v_R/v_P \cos\psi)$ is the focusing effect due to the rupture front motion. The first motion is a jump discontinuity proportional to the stress intensity $K_0$. The first motion (35) was also given by Fossum & Freund (1975) in a much more complicated form.

The first motion at the *S* wave is more complex because of the logarithmic pulse that appears for $\cos\psi < -\kappa^{-1}$. The jump discontinuity at the *S* wave is given by

$$\dot{u}_\psi^S(r, \psi, t) = \frac{K_0}{\mu} v_R \frac{1}{r^{1/2}} \frac{\cos 2\psi}{1 - v_R/v_S \cos\psi} \operatorname{Re}\left[F_S(\psi)\right] H(t - r/v_S) \tag{36}$$

where

$$F_S(\psi) = \frac{\kappa^3}{2(\kappa^2 - 1)} \frac{\cos \psi/2}{(q_R + \kappa \cos \psi) S(\cos \psi/v_S)}.$$

The function $S$ is complex for $-\kappa^{-1} > \cos \psi > -1$. In that zone $S$ should be evaluated slightly above the branch cut between $-v_P^{-1} > p > -v_S^{-1}$ in the complex $p$-plane. Again the function Re $F_S(\psi)$ modifies the radiation pattern cos $2\psi$ from an edge dislocation. The factor cos $\psi/2$ in $F_S$ creates a nodal line along the crack which is not present in dislocations. In the range cos $\psi < -\kappa^{-1}$ there is also a logarithmic pulse at the $S$-wave front

$$\dot{u}_\psi^S(r, \psi, t) = \frac{K_0}{\mu} v_R \frac{1}{r^{1/2}} \frac{\cos 2\psi}{1 - v_R/v_S \cos \psi} \cdot \text{Im}\,[F_S(\psi)] \frac{1}{\pi} \log |t - r/v_S|. \tag{37}$$

It is interesting to note that a logarithmic pulse is the Hilbert transform of a step function. The logarithmic pulse is associated with the *SP* waves guided by the fault.

We can now find the high-frequency radiation associated with the first motions found above. The displacement amplitude spectrum is given by the relatively simple expression

$$|u^i(r, \psi, \omega)| = \frac{K_0}{\mu} v_R \frac{1}{r^{1/2}} R^i(v, \psi) \omega^{-2} \tag{38}$$

where $i = P$, $SV$ or $SH$ and $R^i$ is one of the following radiation patterns

$$R^{SH} = \frac{|\sin \psi/2|}{1 - v_R/v_S \cos \psi}$$

$$R^P = \frac{|\sin 2\psi|}{1 - v_R/v_P \cos \psi} |F_P(\psi)| \tag{39}$$

and

$$R^{SV} = \frac{|\cos 2\psi|}{1 - v_R/v_S \cos \psi} |F_S(\psi)|.$$

The difference between logarithmic and step pulses at the $SV$-wave front disappears in the frequency domain because the logarithmic pulse and the step have the same spectral density. The radiation patterns in (39) are shown in Fig. 6, they differ from those of a suddenly starting dislocation (Ang & Williams 1959) mainly in the backward direction. This difference arises because of the different boundary conditions on the fault plane for a dislocation and a crack model. But the most important difference with a dislocation model is that the spectral amplitude in (38) is related to physical parameters of the rupture front rather than arbitrary slip functions at the fault. The stress intensity factor $K_0$ is a physical property of the crack tip related to the stress drop and the size of the fault.

## 6 Stopping phases and acceleration phases

The starting phases discussed so far are only one of the sources of high-frequency radiation by faulting. In fact, for three-dimensional faults, where rupture nucleates in a small localized zone, a two-dimensional model is not really appropriate for the starting phases. In that case Dahlen (1974) has shown that the starting phases will have an $\omega^{-3}$ behaviour instead of the

$\omega^{-2}$ behaviour of line sources. In most simple models of rupture where the rupture grows at a constant velocity and stops abruptly at a barrier the strongest high-frequency motion is associated with stopping phases (Savage 1966; Madariaga 1976). We can find the radiation from stopping phases making use of the remarkable lack of inertia of cracks. As discussed in Section 2, when a crack suddenly starts to move the stress intensity drops abruptly from $K_0$ to $K_d = K_0 A(v_R)$. Exactly the opposite occurs when a crack stops suddenly, in this case the stress intensity rises from $K_d$ to $K^*$. This happens because $A(v_R)$ is independent of acceleration. Intuitively, we expect that the stopping phase will be of the same form as a starting phase but with a changed sign. A formal proof of this result was given by Eshelby (1969) for antiplane cracks. A similar proof was given by Freund (1972b) for a plane tensional crack that stops abruptly. As we discussed in Section 3 Kostrov (1975) showed that the plane problem may be reduced to a form which is mathematically similar to the antiplane problem. Using this method and Eshelby's proof for antiplane cracks, it may be proven that for inplane shear cracks the radiation of a stopping phase is identical to the radiation of starting phases with a changed sign. Similarly, in the frequency domain, we state without further proof that the absolute displacement spectrum of a stopping phase is also given by (38) with $K^*$ instead of $K_0$.

We have not yet defined $K^*$ for stopping phases. It may be defined as the stress intensity that remains immediately after the rupture velocity drops to zero. This stress intensity may be computed if we know the dynamic stress intensity $K_d$ before the rupture stops, in this case $K^* = K_d / A(v_R)$ from the definition (2). This requires solving the dynamic problem itself. However, we can obtain very good estimates of $K^*$ using the dynamic stress intensities of several solved problems. In general, we find that

$$K_i^* = k_i \overline{\Delta\sigma} L^{1/2} \tag{40}$$

where $K_2^*$ is the in-plane stress intensity, $K_3^*$ is the antiplane intensity, $\overline{\Delta\sigma}$ is the average stress drop on the fault, $L$ is the half-fault length and $k_i$ is a non-dimensional coefficient. In Fig. 7 we plot $k_i$ for self-similar shear cracks. These are cracks that nucleate at a point and expand with constant rupture velocity. Fig. 7 demonstrates the amazing result that $k_i$ is practically independent of rupture velocity so that, very approximately,

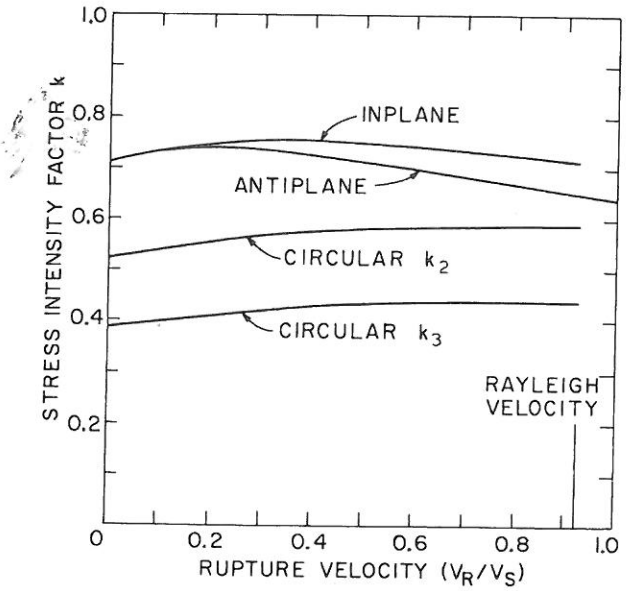


**Figure 7.** Numerical coefficient of the stress intensity factor $K^* = k\,\overline{\Delta\sigma}.\ L^{1/2}$ for plane and antiplane cracks and for circular faults.

$K^* \approx 2^{-1/2} \overline{\Delta\sigma} L^{1/2}$ for two-dimensional cracks. With this value of $K^*$ and (38) we may now obtain the stopping phases for any observation angle. In practice, however, it is very unlikely that the angle $\psi$ will be well known because of uncertainties due to ray bending, scattering, etc. It is interesting then to find an 'average' high-frequency spectrum

$$\langle u^i(r, \psi, \omega)\rangle = \frac{\overline{\Delta\sigma}}{\mu} v_R \left(\frac{L}{r}\right)^{1/2} k_i \langle R^i(v_R)\rangle \omega^{-2}. \tag{41}$$

The average radiation patterns $\langle R^i(v_R)\rangle$ are shown in Fig. 8. We notice that *P* waves are almost unaffected by the rupture velocity while *SH* and *SV* waves are stronger at high rupture velocities due to the focusing effect in the forward direction. The ratio of *S* waves to *P* waves is about 2–3 except at very high velocities. This compares with the well-known ratio $(v_P/v_S)^3 \approx 5.1$ at low frequencies. That is, compared to *S* waves, the radiation of *P* waves is more efficient at high frequencies than at low frequencies. This explains why the *P*-corner frequencies should usually be higher than *S*-corner frequencies.

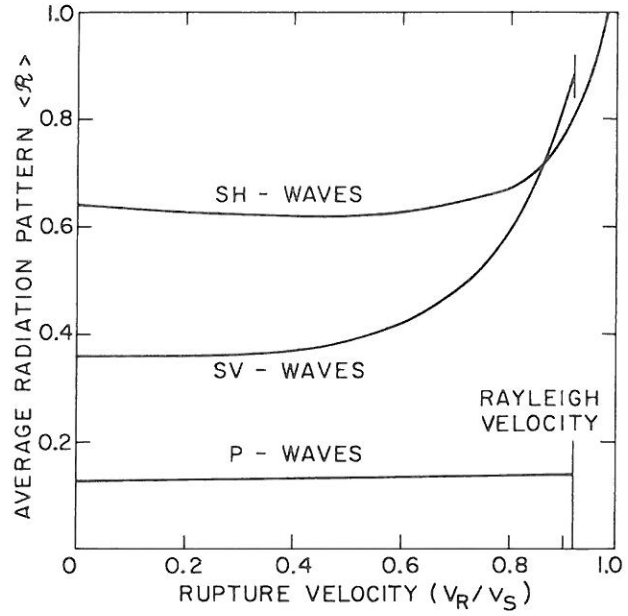


**Figure 8.** Radiation pattern averaged over the angle of radiation $\psi$ as a function of rupture velocity.

The starting and stopping phases discussed so far are distinct radiation instances. For most of the deterministic two dimensional models usually studied they dominate the high-frequency radiation, cause the $\omega^{-2}$ decay at high frequencies and may be used to fix the corner frequencies. We shall apply these results later to a circular fault. In more realistic, although still two dimensional models we should recognize that the strength or fracture energy should be widely variable on a fault plane. Whenever a rupture front encounters a sudden change in strength the rupture velocity would change abruptly. Associated with it there would be a change in the dynamic stress intensity and high-frequency radiation. The radiation from a velocity jump may be evaluated using again the fact that a crack lacks inertia. Then, the radiation is given by

$$|u^i(r, \psi, \omega)| = \frac{K^*}{\mu} \frac{1}{r^{1/2}} \omega^{-2} \cdot Q^i(\psi) \Delta \left[\frac{v_R}{1 - v_R/v_i \cos\psi}\right] \tag{43}$$

where $i$ indicates the type of wave ($P$, $SH$ or $SV$), $v_i$ is the appropriate wave velocity, $\Delta$ indicates the change in the focusing factor due to the rupture velocity change and approximately $K^* \approx 2^{-1/2} \overline{\Delta\sigma} L^{1/2}$. Finally

$$Q^P(\psi) = \sin 2\psi \, |F_P(\psi)|$$
$$Q^{SV}(\psi) = \cos 2\psi \, |F_S(\psi)| \tag{44}$$

and

$$Q^{SH}(\psi) = \sin \psi/2.$$

One can envision many of these velocity jumps, each radiating like (43). This is a source of incoherent radiation not incorporated in deterministic models.

The results obtained so far describe the high-frequency radiation from abrupt changes in rupture velocity. In reality the strength on the fault probably changes continuously at least in some small scale. In this case the results we have obtained are asymptotic approximations for the radiation at wavelengths longer than the distance over which the strength and the rupture velocity change. In this sense, we may comment on Dahlen's (1974) result that stopping phases should be weaker than starting phases if the rupture velocity varies continuously. This statement is strictly valid only at very high frequencies, such that the wavelengths are shorter than the deceleration time at the stopping of rupture. For longer wavelengths but still shorter than the corner frequency the acceleration and deceleration appear to be sudden and the radiation approximates the results obtained for velocity jumps. In this range of frequencies the stopping phases are stronger than the starting phases and they have an $\omega^{-2}$ frequency dependence.

One is tempted to extend our results to wavelengths such that the continuous variation of the rupture velocity is important. In this case we may approximate the rupture propagation by a series of discrete jumps in velocity and sum the radiation from each jump. It is difficult to justify this procedure, however, since our previous results are strictly valid only for discrete wavefronts. An analysis of that problem is beyond our present purposes. What we want to stress, however, is that the stopping and starting phases provide strong upper bounds to the radiation of high frequencies and the $\omega^{-2}$ frequency dependence is the slowest possible spectral decay at high frequencies.

## 7 Radiation from faults in three dimensions

So far we have considered only two-dimensional fault models. These models should be appropriate in the vicinity of the fault, but as we move away from the fault the finiteness and shape of the fault play an increasingly important role. A general analysis of three dimensional cracks poses some analytical problems. However, under some circumstances we may use Keller's (1962) geometrical theory of diffraction to extend our two dimensional solutions into three dimensions. These methods have been used by Ahluwalia, Keller & Jarvis (1974) to study some three dimensional displacement boundary value problems. We consider wavelengths which are much shorter than the radius of curvature of the rupture front. In this case the elastodynamic field in the vicinity of the rupture front is essentially two dimensional with components of both plane and antiplane slip. The rupture front again lacks inertia and abrupt rupture velocity jumps are likely. Rupture velocity variation generates changes in stress intensity and radiation of high-frequency elastic waves.

Let us consider the radiation from a segment of rupture front which changes velocity abruptly and simultaneously (see Fig. 9). If the wavelength is shorter than $\rho$, the main effect

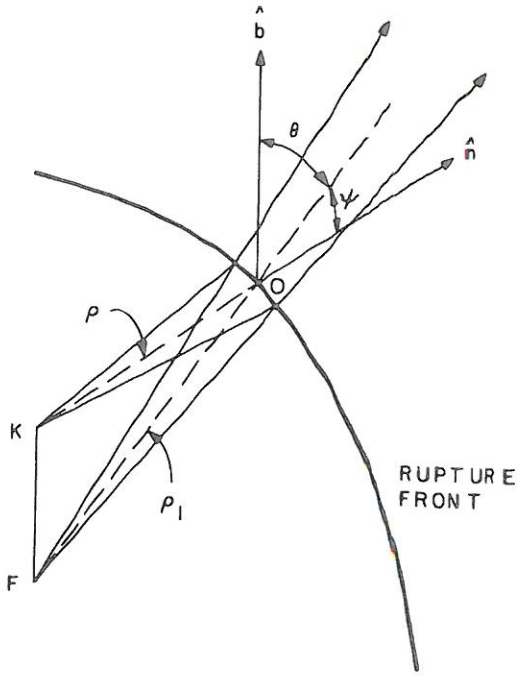


**Figure 9.** Geometry of radiation from a curved rupture front. The radius of curvature of the rupture front at 0 is $\rho$. Radiation from the vicinity of 0 is similar to two-dimensional radiation except that the rays diverge from the focal point F. F is on a line normal to the crack plane through the centre of curvature K. $\hat{n}$ and $\hat{b}$ are the normal and binormal to the rupture front, respectively.

of the curvature of the rupture front is to produce additional geometrical spreading of the radiated waves. As shown by Keller (1962) we obtain the three-dimensional radiation by replacing the cylindrical geometrical spreading factor $r^{-1/2}$ by

$$R^{-1/2}(1 + R/\rho_1)^{-1/2} \tag{45}$$

where, referring to Fig. 9, $\rho_1 = \rho/\sin\theta$ and $R$ is the distance measured from the rupture front. Thus, when $R \to 0$ the spreading is cylindrical, but as we move away from the fault into the far field ($R \gg \rho_1$) the radiation appears more and more spherical and the geometrical decay takes the form $R^{-1}$ typical of spherical waves. Since all the other dynamical properties of two-dimensional waves remain valid we may write the radiation from a sudden velocity change in the form

$$|u^i(R, \theta, \omega)| = \frac{K_i^*}{\mu} \frac{1}{[R(1 + R\sin\theta/\rho)]^{1/2}} \cdot \frac{1}{\omega^2} \cdot Q^i(\psi)\Delta \left[\frac{v_R}{1 - v_R/v_i \cos\psi}\right] \tag{46}$$

where $K_i^*$ is the appropriate stress intensity factor, i.e. the antiplane stress intensity for *SH* waves or the in-plane intensity for *P* and *SV* waves. $\psi$ is the angle between the direction of observation and the outward normal $\hat{n}$ to the rupture front (see Fig. 9). The functions $Q^i(\psi)$ were defined in equation (44) of the previous section.

Equation (46) indicates that the rupture front acts like a radiator emitting tube-like wavefronts centred around the rupture front. The strongest high frequency radiation occurs when the rupture front changes abruptly its rupture velocity, for instance when it starts moving or when it stops at an unbreakable region. As in two-dimensional models, the stress intensity $K^*$ is proportional to the stress drop and the square root of some characteristic size of the fault, but it should also include the angle that the slip direction makes with the rupture front.

The previous results are only approximately valid since we assumed that some section of the rupture front changes its velocity simultaneously. In general, however, we may expect that the rupture velocity change will initiate at the point on the rupture front that first comes in contact with the variable strength region. Neighbouring points on the rupture front will change their rupture velocity after some delay. As a consequence the radiated wave fronts will be smoother than in the simultaneous situation we have considered here. The effect of this complication will be deferred for some future work. However, we note that the effect of non-simultaneous rupture velocity changes and of smooth rupture velocity change are similar in that they will affect the spectrum only beyond a certain frequency associated with the time that it takes to change the rupture velocity. This time must be considerably shorter than the corner periods associated with source dimensions. Therefore our results are upper bounds to the high frequency radiation due to acceleration or deceleration of the rupture front.

## 8 High-frequency radiation from a circular fault

In Madariaga (1976) we studied numerically the problem of a circular shear fault that grows self-similarly at a constant rupture velocity and stops abruptly in all its rupture front when the radius is $a$. This model provides a unique opportunity to verify the numerical results with the present theory. We can use the results of the previous section because the rupture stops simultaneously. The high-frequency radiation is dominated by the stopping phases radiated by the edge of the fault when rupture stops abruptly. The solution before stopping was obtained by Kostrov (1964). From this solution we find the velocity intensity factor defined in equation (3).

$$V_{xd} = \sqrt{2}\frac{\Delta\sigma a^{1/2}}{\mu} v_S C \tag{47}$$

where the subscript index $x$ indicates that the slip velocity in the $x$ direction, $\Delta\sigma$ is the stress drop and $C$ is a constant that depends on the rupture velocity (Dahlen 1974). We can split $V_{xd}$ into a plane and an antiplane velocity concentration and then use (4) to find

$$\begin{aligned} K_3^* &= \Delta\sigma a^{1/2} k_3 \sin\phi \\ K_2^* &= \Delta\sigma a^{1/2} k_2 \cos\phi \end{aligned} \tag{48}$$

where $\phi$ is the azimuth on the fault plane measured from the $x$ axis. The numerical factors

$$k_i = C(v_S/v_R)\, B_i(v_R) 2^{-1/2} \tag{49}$$

are plotted on Fig. 7, $B_i(v_R)$ indicates either the in-plane or antiplane functions defined after (4). As in the plane cases the $k_i$'s are almost independent of rupture velocity. The coefficient $k_2$ is very approximately (4/3) $k_3$ when $v_P = 3^{1/2} v_S$.

We may now write the far-field stopping phases using the results of the previous section, we find

$$|u^i(R, \theta, \phi, \omega)| = \frac{\Delta\sigma a}{\mu} k_i v_R \cdot \frac{\mathscr{R}^i}{R}\frac{1}{\omega^2} D^i\left(\frac{\pi}{2} - \theta\right) \frac{1}{1 - (v_R/v_i)\sin\theta} \tag{50}$$

where $i$ indicates $P$, $SV$ or $SH$ waves, $\mathscr{R}^i$ is the appropriate double-couple radiation pattern, $k_i$ indicates $k_2$ for $P$ and $SV$ waves and $k_3$ for $SH$ waves. The $SH$ waves have motion parallel to the edge of the fault and $SV$ waves have motion in a plane perpendicular to the edge. The

diffraction factors $D^i(\psi)$ are defined by

$$D^P(\psi) = |F_P(\psi)|\ |\cos\psi|^{-1/2}$$

$$D^{SV}(\psi) = |F_S(\psi)|\ |\cos\psi|^{-1/2} \tag{51}$$

$$D^{SH}(\psi) = (2\cos\psi/2)^{-1}\,|\cos\psi|^{-1/2}$$

where $\psi$ is the angle between the direction of the observer and the outer normal to the fault edge. $F_p(\psi)$ and $F_S(\psi)$ were defined in (35) and (36) respectively.

At any point in the far-field there will be two stopping phases arriving from the nearest and farthest point on the fault. Equation (50) defines the radiation from the nearest point, radiation from the farthest point is simply obtained replacing $(\pi/2 - \theta)$ by $(\pi/2 + \theta)$ in (50). These two stopping phases will interfere creating a series of holes in spectrum as seen in Fig. 10. We are interested in the general trend at high frequencies rather than in the details of the spectrum, so that we can estimate the high frequencies by the average square of the spectral amplitudes of the two stopping phases

$$|u(R,\theta,\phi,\omega)| = (|u(R,\theta,\phi,\omega)|^2 + |u(R,\theta,\pi+\phi,\omega)|^2)^{1/2} \tag{52}$$

In Fig. 10 we show an example of numerically computed far field waves radiated by a circular fault with rupture velocity $v_R = 0.9\,v_S$. The angle of radiation is $\theta = 60^\circ$. In the time domain pulses we have indicated with arrows the arrival times of the stopping phases. Our theoretical results predict slope changes in the displacement pulses of the time of arrival of the stopping phases. These slope changes have been smoothed by the numerical solution.

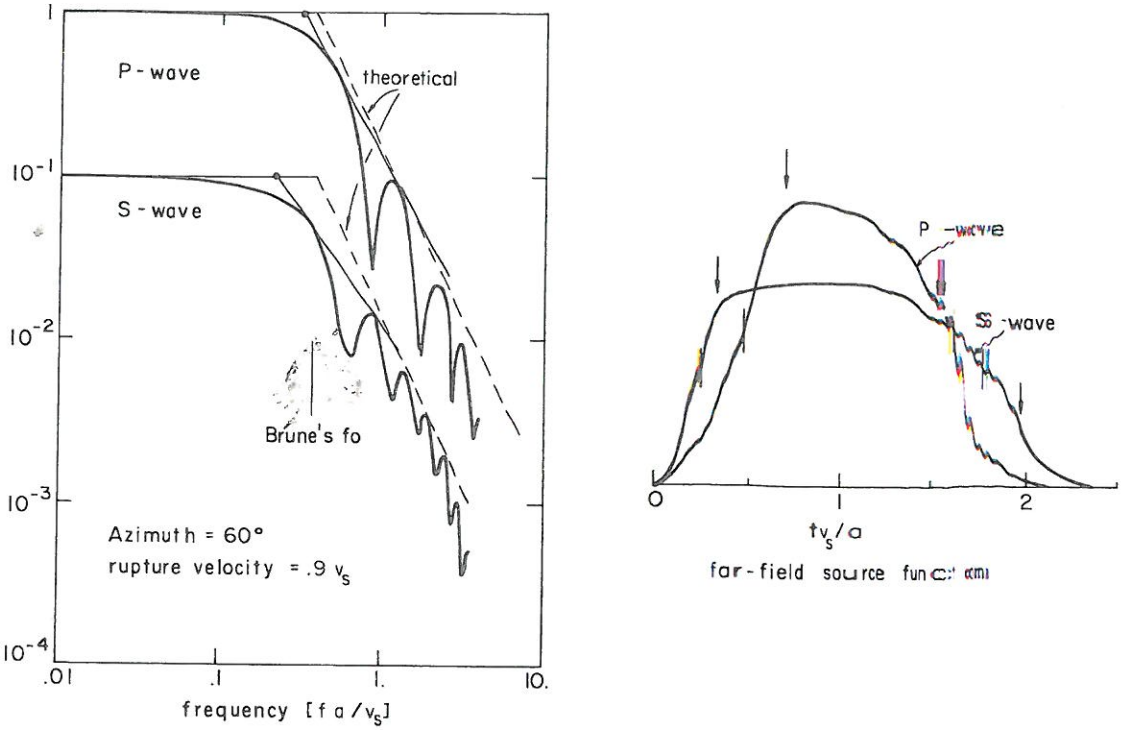


Figure 10. Numerical solution of the far-field radiation by a subsonic circular fault. Rupture velocity $v_R = 0.9\,v_S$. The arrows above the time-domain source functions indicate the arrival of stopping phases. In the spectrum we indicate with dashed lines the high frequencies asymtotes estimated by (50). The dots indicate the numerical corner frequencies obtained from the interception of the low-frequency asymptote and the intermediate frequency trend (thin solid line).

In the same figure we show the displacement spectrum obtained from the numerical solution of the circular fault (Madariaga 1976) and we indicate with dashed lines the theoretical estimates of the $SV$ high-frequency spectrum. The agreement between the analytical and numerical solutions is excellent. This confirms our contention that in the circular model the radiation of high frequencies is controlled entirely by the stopping phases. From the point of view of high-frequency generation a circular fault with constant rupture velocity appears as a circular line coincident with the final edge of the fault. There is no high frequency radiation while rupture proceeds at constant rupture velocity. There is also a weak ($\omega^{-3}$) starting phase emitted during nucleation.

In Fig. 10 we have also indicated the corner frequencies computed as in Madariaga (1976) by the intersection of the low frequency and intermediate frequency trends indicated by solid lines. These numerical corner frequencies differ somehow from the corner frequencies that would be obtained using the theoretical high-frequency trend. We may compute the theoretical corner frequencies as the intersection of the high-frequency asymptote (52) and the low-frequency asymptote given by the well-known relation

$$|u^i(R, \theta, \phi, \omega)| = \frac{4}{7\pi\rho v_i^3} \Delta\sigma a^3 \frac{\mathscr{R}^i}{R}$$

where $i$ indicates the type of wave, $\rho$ is the density and the rest of the variables are the same as those defined in equation (50). The corner frequencies $\omega_0^i$ (radian/s) are given by

$$\left(\frac{\omega_0^i a}{\beta}\right)^2 = \frac{7\pi}{4} k_i \frac{v_R v_i^3}{v_S^4} \cdot \left( \frac{|D^i(\pi/2 - \theta)|^2}{(1 - (v_R/v_i)\sin\theta)^2} + \frac{|D^i(\pi/2 + \theta)|^2}{(1 + (v_R/v_i)\sin\theta)^2} \right)^{1/2} \tag{53}$$

where $i$ indicates $P$, $SV$ or $SH$ waves, $v_i$ is the appropriate wave velocity and the other variables were defined in (50). The theoretical corner frequencies for the case $v_R = 0.75\, v_S$ are shown in Fig. 11 as a function of polar angle $\theta$. In the same figure we plot the numerical corner frequencies computed for a few values of $\theta$. In the numerical solutions we forced the $SV$ and $SH$ radiation to be identical in order to reduce the problem to two dimensions. Although at high frequencies the $SH$ and $SV$ radiation are slightly different, these differences are numerically insignificant in the frequency range in which the numerical method is appropriate. The theoretical $SV$ corner frequencies show a peak at $\sin\theta = v_S/v_P$ due to the strong coupling between $P$ and $SP$ waves. The peak in corner frequency near $\theta = 0^\circ$ are due to the strong focusing of radiation in the direction normal to the fault. As $\theta \to 90^\circ$ the theoretical corner frequencies depart from the numerical ones due to the focusing of high frequencies at shallow angles to the fault plane. In this range these are significant intermediate frequency slopes as shown in Fig. 10 or in the spectra shown in Madariaga (1976). The numerical corner frequencies were computed using the intermediate slopes rather than the $\omega^{-2}$ high-frequency slope.

## 9 Conclusions

We have presented a theory for the high-frequency radiation by two-dimensional stress-drop (shear crack) models of earthquakes. In these models the fault is prescribed as a planar region in which the stress drops from the tectonic stress to the kinematic friction while slip is taking place. These models are identical to dynamic shear crack models in which the stress drop is prescribed inside the fault. The most significant feature of crack models is

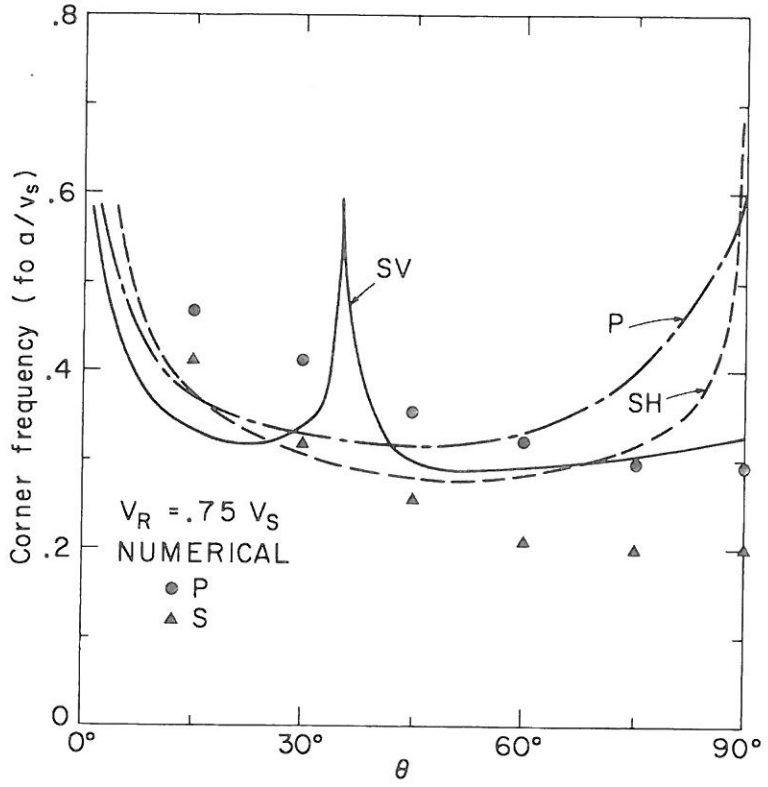


**Figure 11.** Far-field corner frequencies of the circular fault as a function of polar angle $\theta$. The rupture velocity is $v_R = 0.75\, v_S$. The lines were computed using the present theory and dots were obtained numerically by Madariaga (1976).

the presence of strong stress concentrations in the vicinity of the edge of the fault. When the fault is extending there are also slip velocity concentrations behind the rupture front; the largest values of slip velocity on the fault occur precisely at these concentrations. Since the radiation of high frequencies (or first motions of discontinuous phases) is controlled by the slip velocity on the fault, we expect that from the point of view of high frequencies the rupture front is the main source of radiation. Radiation is emitted only when the rupture front is accelerating or decelerating due to changes in the stress concentration (load of the crack tip) or to changes in the strength of the fault. An upper bound to the high-frequency radiation is given by abrupt changes in rupture velocity, for instance stopping phases. In two dimensions these phases are cylindrical wave fronts on which the slip velocity has step changes or weak logarithmic singularities. The frequency-dependence of the displacement radiation is, therefore, of the $\omega^{-2}$ type. This is the highest possible asymptotic trend at high frequencies. When the rupture velocity changes are smooth we expect that the $\omega^{-2}$ will give an upper bound to the radiation. Beyond a certain frequency associated with the total time of acceleration or braking the high-frequency decay will be less than $\omega^{-2}$ and will depend on the details of the acceleration.

These two-dimensional results may be extended to three dimensions when the rupture front accelerates simultaneously at least on a certain segment. This is the case of the self-similar circular fault that grows at constant velocity and stops abruptly. In this highly symmetrical case the stopping phases control the radiation and the present theoretical predictions agree extremely well with the numerical solution that we obtained in Madariaga (1976).

But in real three-dimensional faults it is quite unlikely that the velocity changes will occur simultaneously on the rupture front. We can postulate the following model of high-

frequency generation. The rupture front acts as a generalized moving curvilinear source. It emits high-frequency radiation only when it is accelerating or decelerating. We expect that these rupture velocity changes will be produced in response to variations in the strength (or cohesion) of the fault. When the rupture front encounters a high-strength region the rupture velocity will decrease more or less abruptly generating strong high-frequency phases. The rupture velocity will change starting from the point on the rupture front that first encounters the high-strength region. The rupture velocity change will 'propagate' laterally from this point along the rupture front. Radiation from such a velocity change will be weaker than $\omega^{-2}$ for frequencies higher than a certain threshold probably associated with the time of spreading of the rupture velocity change along the rupture front. The study of these fully three-dimensional effects goes beyond the scope of the present work but needs further examination.

## Acknowledgments

I thank Professor N. Toksöz for his continuous support and encouragement. This work was sponsored by the Division of Earth Sciences of the National Science Foundation under grant EAR75-14808 A01.

## References

Acton, F. S., 1970. *Numerical methods that work*, Harper and Row, New York..

Achenbach, J. D., 1974. On dynamic effects in brittle fracture, in *Mechanics today*, Pergamon Press, New York.

Achenbach, J. D., 1975. *Wave propagation in elastic solids*, North-Holland/American Elsevier, Amsterdam, Holland.

Ahluwalia, D. S., Keller, J. B. & Jarvis, R., 1974. Elastic waves produced by surface displacements, *SIAM, J. appl. Math.*, **26**, 108–119.

Aki, K., 1967. Scaling law of seismic spectrum, *J. geophys. Res.*, **72**, 1217—1231.

Andrews, D. J., 1976. Rupture velocity of plane-strain shear cracks, *J. geophys. Res.*, **81**, 5679–5687.

Ang, D. D. & Williams, M. L., 1959. The dynamic stress field due to an extensional dislocation, *4th Midwestern Conference on Solid Mechanics*, University of Texas.

Ben-Menahem, A., 1962. Radiation of seismic body waves from a finite moving source in the earth, *J. geophys. Res.*, **67**, 345–350.

Brune, J. N., 1970. Tectonic stress and the spectra of seismic shear waves from earthquakes, *J. geophys. Res.*, **75**, 4997–5009.

Burridge, R., 1969. The numerical solution of certain integral equations with non-integrable kernels arising in the theory of crack propagation and elastic wave diffraction, *Phil. Trans. R. Soc. Lond. A*, **265**, 353.

Burridge, R., 1973. Admissible speeds for plane-strain self-similar shear cracks with friction but lacking cohesion, *Geophys. J. R. astr. Soc.*, **35**, 439–455.

Dahlen, F. A., 1974. On the ratio of *P*-wave to *S*-wave corner frequencies for shallow earthquake sources, *Bull. seism. Soc. Am.*, **64**, 1159–1180.

Das, S., 1976. A numerical study of rupture propagation and earthquake source mechanism, *Thesis*, M.I.T., Cambridge, Massachusetts.

de Hoop, A. T., 1958. Representation theorems for the displacement in an elastic solid and their application to elastodynamic diffraction theory, *Doctoral dissertation*, Delft.

Eshelby, J. D., 1969. The elastic field of a crack extending non-uniformly under general anti-plane loading, *J. Mech. Phys. Solids*, **17**, 177–179.

Fossum, A. F. & Freund, L. B., 1975. Non-uniformily moving shear crack model of a shallow focus earthquake mechanism. *J. geophys. Res.*, **80**, 3343—3347.

Freund, L. B., 1972a. Crack propagation in an elastic solid subject to general loading, II. Non-uniform rate of extension, *J. Mech. Phys. Solids*, **20**, 141–152.

Freund, L. B., 1972b. Energy flux into the tip of an extending crack in an elastic solid, *J. Elasticity*, **2**, 341–348.

Freund, L. B., 1976. The analysis of elastodynamic crack tip stress fields in *Mechanics Today vol 3*, pp. 55–91, ed. Nemat-Nasser, S., Pergamon Press, New York.

Haskell, N. A., 1964. Total energy and energy spectral density of elastic wave radiation from propagating faults, *Bull. seism. Soc. Am.*, **54**, 1811–1841.

Haskell, N. A., 1966. Total energy and energy spectral density of elastic wave radiation from propagating faults. Part II. A statistical source model, *Bull. seism. Soc. Am.*, **56**, 125–140.

Husseini, M. I., Jovarovich, B. B., Randall, M. J. & Freund, L. B., 1975. The fracture energy of earthquakes, *Geophys. J. R. astr. Soc.*, **43**, 367–385.

Keller, J. B., 1962. Geometrical theory of diffraction, *J. opt. Soc. Am.*, **52**, 116–130.

Kostrov, B. V., 1964. Self-similar problems of propagation of shear cracks, *J. appl. Math. Mech.*, **28**, 1077–1087.

Kostrov, B. V., 1966. Unsteady propagation of longitudinal shear cracks, *J. appl. Math. Mech.*, **30**, 1241–1248.

Kostrov, B. V., Nikitin, L. V. & Flitman, L. M., 1970. Mechanics of brittle fracture, *Izv. Akad. Nauk SSSR, Mekh, Tverd. Telo.*, **3**.

Kostrov, B. V., 1975. On the crack propagation with variable velocity, *Int. J. Fracture Mech.*, **14**, 47–56.

Madariaga, R., 1976. Dynamics of an expanding circular fault, *Bull. seism. Soc. Am.*, **65**, 163–182.

Rice, J. R., 1968. Mathematical analysis in the mechanics of fracture, in *Fracture: an advanced treatise*, vol. 2, pp. 191–311, ed. Liebowitz, H., Academic Press, New York.

Rice, J. R. & Simons, D. A., 1976. The stabilization of spreading shear faults by coupled deformation–diffusion effects in fluid-infiltrated porous materials, *J. geophys. Res.*, **81**, 5322–5334.

Richards, P. G., 1976. Dynamic motions near an earthquake fault: a three-dimensional solution, *Bull. seism. Soc. Am.*, **66**, 1–32.

Savage, J. C., 1966. Radiation from a realistic model of faulting, *Bull. seism. Soc. Am.*, **56**, 577–592.

Thau, S. A. & Lu, T. H., 1971. Transient stress intensity factors for a finite crack in an elastic solid caused by a dilatational wave, *Int. J. Solids Structures*, **7**, 731–750.

## Appendix 1: the function $S(p)$

The function $S(p)$ was introduced by de Hoop (1958) in his study of elastic wave diffraction by plane cracks. The function arises from a Wiener–Hopf factorization of the Rayleigh function (21). It is defined by

$$S(p) = \exp\left[-\frac{1}{\pi}\int_1^{\kappa} \tan^{-1}\left(\frac{\xi^2\gamma_P\gamma_S}{(\kappa^2/2-\xi^2)^2}\right)\frac{d\xi}{\xi + v_P p}\right] \tag{A1}$$

where

$\gamma_P = (\xi^2 - 1)^{1/2}$

$\gamma_S = (\kappa^2 - \xi^2)^{1/2}$

and

$\kappa = v_P/v_S$.

The evaluation of $S(p)$ is very inconvenient in the form (A1). In fact, in the half-plane Re $p > 0$, $S(p)$ varies from a minimum $S(0) = 0.79622$ to a maximum $S(\infty) = 1$ (assuming $\kappa = 3^{1/2}$). In this half plane, for small $|p|$, it is convenient to use a rational approximation

given in Thau & Lu (1971). For large $|p|$ we use a Laurent series expansion for the exponent

$$S(p) = \exp\left[-\frac{1}{\pi}\sum_i b_i p^{-i}\right] \tag{A2}$$

where $b_1 = 0.9383265$, $b_2 = 1.255123$, $b_3 = 1.712679$, $b_4 = 2.382243$ and $b_5 = 3.373985$.

In the half plane Re $p < 0$, we use the definition (21) in order to find $S(p)$ in terms of $S(-p)$.

## Appendix 2: stress due to the sudden start of a plane crack

The function $T(\tau)$ introduced in (29) is given by

$$T(\tau) = \frac{1}{\pi}\int_1^\tau \frac{(q_R - q)}{(M-q)} \frac{\text{Im}\,[S(-q/v_P + i0)]}{[(\kappa - q)(\tau - q)]^{1/2}}\, dq \tag{A3}$$

for $\kappa > \tau > 1$, where $q_R = v_P/c_R$, $M = v_P/v_R$ and Im denotes imaginary part, $v_P$ and $c_R$ denote $P$ and Rayleigh wave velocities respectively.

$$T(\tau) = \frac{M - q_R}{(M-\kappa)^{1/2}} \frac{S(-1/v_R)}{(M-\tau)^{1/2}} - 1 \qquad \text{for } M > \tau > \kappa$$

and

$$T(\tau) = -1 \qquad \text{for } \tau > M$$

## Appendix 3: slip velocity due to sudden start of plane crack

The non-dimensional velocity function $U(\tau)$ introduced in (31) is given by

$$U(\tau) = \frac{1}{(q_R + M)} \frac{(\kappa + M)^{1/2}}{S(1/v_R)(\tau + M)^{1/2}}$$

for $x < 0$, $\tau > q_R$;

$$U(\tau) = \frac{1}{(q_R + M)}\left[\frac{(\kappa + M)^{1/2}}{S(1/v_R)(\tau + M)^{1/2}} - \frac{(q_R - \kappa)^{1/2}}{S(-1/c_R)(q_R - \tau)^{1/2}}\right]$$

for $x < 0$, $q_R > \tau > \kappa$;

$$U(\tau) = -\frac{1}{\pi}\int_1^\tau \frac{dq}{(M+q)(q_R - q)} \frac{(\kappa - q)^{1/2}}{(\tau - q)^{1/2}} \text{Im}\,[S^{-1}(-q/v_P + i0)]$$

for $x < 0$ and $\kappa > \tau > 1$;

and

$$U(\tau) = \frac{1}{q_R + M} \cdot \frac{(\kappa + M)^{1/2}}{S(1/v_R)} \cdot \frac{1}{(\tau - M)^{1/2}}$$

for $x > 0$, $\tau > M$.

**Appendix 4: radiation from a plane crack**

The non-dimensional functions $V_i(\tau, \psi)$ introduced in (33) may be separated into $P$, $S$ and $SP$ contributions.

For $P$ waves we get

$$V_i^P(\tau, \psi) = \frac{1}{2(\kappa^2 - 1)\pi} \int_1^\tau \frac{d\xi}{[(\tau - \xi)(\xi^2 - 1)]^{1/2}} \operatorname{Re}\,[D(p)G_i(p)]$$

where $p(\xi)$ is the Cagniard contour for $P$ waves

$$p(\xi) = -\xi \cos\psi + i\eta_P \sin\psi, \quad -\pi \leqslant \psi \leqslant \pi$$

and

$$\eta_P(\xi) = (\xi^2 - 1)^{1/2}$$

The function $D(p)$, given by

$$D(p) = \frac{(\kappa - p)^{1/2}}{(M + p)(q_R - p)S(-p/v_P)}$$

is a common factor that appears in $P$, $S$ and $SP$ waves.

Finally

$$G_x(p) = 2p^2(1 - p^2)^{1/2}$$

$$G_z(p) = -2p(1 - p^2).$$

For $S$ waves we get

$$V_i^S(\tau, \psi) = \frac{1}{2(\kappa^2 - 1)\pi} \int_\kappa^\tau \frac{d\xi}{[(\tau - \xi)(\xi^2 - \kappa^2)]^{1/2}} \operatorname{Re}\,[D(p)G_i(p)]$$

where the Cagniard contour $p(\xi)$ is the same as that for $P$ waves, but with $\eta_S = (\xi^2 - \kappa^2)^{1/2}$ instead of $\eta_P$. The function $D(p)$ is the same as above and

$$G_x(p) = (\kappa^2 - 2p^2)(\kappa^2 - p^2)^{1/2}$$

$$G_z(p) = (\kappa^2 - 2p^2)p.$$

The $SP$ waves appear only in a wedge-like zone in the backward quadrant $\cos\psi < -\kappa^{-1}$.

$$V_i^{PS}(\tau, \psi) = \frac{1}{2(\kappa^2 - 1)\pi} \int_{\tau_{ps}}^{\min(\tau,\kappa)} \frac{d\xi}{[(\tau - \xi)(\kappa^2 - \xi^2)]^{1/2}} \operatorname{Im}\,[D(p)G_i(p)]$$

where the Cagniard contour is

$$p(\xi) = -\xi \cos\psi - (\kappa^2 - \xi^2)^{1/2} \sin\psi.$$

The functions $D(p)$ and $G_i(p)$ are the same as those for $S$ waves. The arrival time of $SP$ waves is given by

$$\tau_{ps} = |\cos\psi| + (\kappa^2 - 1)^{1/2} \sin\psi$$

which is the travel time of a wave that leaves the tip as an $S$ wave along the fault and is then refracted at the critical angle as a $P$ wave. The evaluation of the integrals was done numerically, eliminating previously the singularities by trigonometric transformation (Acton 1970).